JOURNAL OF MECHANICAL ENGINEERING AND SCIENCES (JMES)
ISSN: 2289-4659 e-ISSN: 2231-8380
VOL. 16, ISSUE 1, 8662 – 8672
DOI: https://doi.org/10.15282/jmes.16.1.2022.02.0685

ORIGINAL ARTICLE

Numerical investigation of inlet opening size on wind-driven cross ventilation

L.K. Moey[1], Y.H. Sing[2], V.C. Tai[1], T.F. Go[3], J.Y. Ng[1]

[1] Centre for Modelling and Simulation, Faculty of Engineering, Built Environment & Information Technology, SEGi University, 47810, Selangor, Malaysia
Phone: 03-6145 1777; Fax.: 03-6145 1666
[2] Faculty of Engineering, Built Environment & Information Technology, SEGi University, 47810, Selangor, Malaysia
[3] Centre for Advanced Materials and Intelligent Manufacturing, Faculty of Engineering, Built Environment & Information Technology, SEGi University, 47810, Selangor, Malaysia

ABSTRACT – The purpose of this study is to investigate the effect of opening size on indoor airflow characteristics of a naturally ventilated building model. The numerical simulation based on 3D-steady RANS equation was performed in this study. A total of five different inlet to outlet opening ratios, namely 1:4, 1:2, 1:1, 2:1 and 9:4 were included in the study and analysed. The results of model validation and grid independence analysis were consistent with the previous study. The simulation results in this study are discussed based on the velocity vector, velocity and pressure, pressure drop and ventilation rate. Through the study, the results have clearly illustrated that the velocity vector, velocity and pressure, pressure drop and ventilation rate are highly dependent on the opening ratio. When air passes through the building model, it forms a recirculation at the top and bottom of the airflow. In addition, the contours of velocity and pressure have indicated that the lower the opening ratio, the higher the velocity and subsequently lower pressure inside the building model. For the pressure drop, the results have shown that the lower the opening ratio, the higher the pressure drop. Beyond that, when the opening ratio is less than 1, the ventilation rate was increased but when the opening ratio greater than 1, the ventilation rate begins to decrease. Therefore, change in the size of inlet opening will greatly affect the performance of ventilation rate.

ARTICLE HISTORY
Received: 14th June 2021
Revised: 17th Sept. 2021
Accepted: 29th Sept. 2021

KEYWORDS
Indoor airflow characteristics;
3D-steady Rans equation;
opening ratio;
velocity vector;
pressure drop;
ventilation rate

INTRODUCTION

Ventilation is a process of continuously replacing the air in an enclosed space with the external environment, thereby eliminating polluted air that may be harmful to the human body, and obtaining good indoor air quality and thermal comfort [1]. Ventilation can be divided into two types, namely natural ventilation and mechanical ventilation. Natural ventilation used natural forces such as wind to achieve ventilation [2]. However, mechanical ventilation uses fans, air conditioning or other mechanical devices in the building to achieve ventilation. Due to the use of mechanical devices, it has caused an increase in energy consumption. According to the report by World Business Council for Sustainable Development (WBCSD), the building accounts for 40% of the world's energy consumption in order to provide a building with thermal comfort. In addition, the report also pointed out that the carbon emission of buildings is even higher than the transportation sector [3]. Increasing in energy consumption and carbon emissions from buildings has resulted in an increase in temperature, harming both the environment and human health. Hence, the implementation of natural ventilation is very important. It is an alternative method that can be used to reduce energy consumption and protect the environment and subsequently protect the environment and human health [4].

Natural ventilation can be categorized into three different methods, namely single-sided ventilation, cross ventilation and stack ventilation [5,6]. Single-sided ventilation has only one or more openings on the same façade wall to generate air circulation [7]. However, the cross ventilation contains two windows located opposite to each other. The side with the wind is called the windward facade, and the opposite side that faces away from the wind is called the leeward facade. Cross ventilation can be driven by wind or buoyancy. Therefore, when the windows on the windward and leeward facade have identical height, the wind is the main natural driving force. Moreover, Thermal buoyancy is only generated when the windows on the windward and leeward facade have different heights [5]. Stack ventilation, on the other hand, has an opening at the bottom that allows air to enter and then the air will flow out through openings at the top of the building such as roofs or vents. The driving force for stack ventilation comes from thermal buoyancy [6].

Boundary Layer Wind Tunnel (BLWT) is one of the wind tunnel tests that is commonly used in the study of natural ventilation. Karava et. al. used BLWT to assess the internal pressure coefficients and discharged coefficients of buildings [8]. The cross ventilation of the building was caused by sliding window openings on two adjacent windows. This study found that internal pressure coefficients and discharge coefficients of cross ventilation varying greatly with the ratio of the inlet to outlet and opening area. Moreover, when the porosity of the windward wall is higher than 10%, the internal pressure coefficient is not uniform. In short, the opening ratio of the inlet to outlet is an important parameter for analyzing ventilation problems.

*CORRESPONDING AUTHOR | L. K. Moey | ✉ moeylipkean@segi.edu.my

A CFD model has been used to investigate the ventilation effectiveness of building under different wind incidence angles with various inlet opening areas [9]. In this study, three different inlet opening areas were considered. It was found that when the wind blows perpendicular to the building, the ventilation rate will not reach the maximum, due to the airflow will leave the building through a short circuit. However, due to the formation of two wind-driven vortices in the building, the uniformity of ventilation is highest when the wind blows vertically toward the building. The study also shows that when the wind incident angle is in the range of 10°-40°, the environmental heterogeneity is highest. In addition, it was also found that in some cases, the ventilation rate determined by the flow through the opening of the building may not accurately represent the actual ventilation rate of the building, and measurement of pollutant attenuation can obtain more accurate ventilation rate measurement. Besides, Visagavel and Srinivasan performed simulations to study the air velocity in the cross and single ventilation [10]. Different sizes of openings at a specific height of the wall were used in this simulation. The turbulence model of Reynolds-averaged Navier Stokes (RANS) was chosen for this study. The results indicated that cross ventilation is always more effective than single-sided ventilation. In addition, the study by Moey et. al. also demonstrated that the airflow rate increases as the width of the opening increases [11].

Through the literatures, it has been revealed that the opening size is a critical parameter because the change of opening size will greatly affect the ventilation effect of the building. Furthermore, the studies showed that the ventilation performance of cross ventilation is always better than single-sided ventilation [10]. Therefore, the cross-ventilated isolated building is used and the size of the opening is the focus of this study. The opening size can be further investigated to improve the performance and influence of opening size on cross ventilation. The other parameters such as velocity vector, ventilation rate and pressure can also be further analysed to understand the indoor airflow characteristics under various opening sizes. Through this study, the appropriate opening size of cross ventilation can be determined and further insight into the influence of ventilation performance under various opening sizes. Hence, the numerical simulation was used to examine the influence of opening size on cross ventilation of the isolated building.

This paper is further divided into several different sections, namely section 2, section 3 and section 4. In section 2, the information of numerical simulation will be discussed in detail such as model validation, boundary condition, grid independence analysis, computational domains, solver settings and model geometries. Moreover, in section 3, the numerical simulation results under various opening ratios will be discussed. Finally, conclusions about the study will be presented in section 4.

NUMERICAL STUDY

Model Geometry

In this study, an isolated building model was used to investigate the indoor airflow characteristics. The dimension of the building model was 100 mm x 100 mm x 80 mm (length x width x height), which is the reduced scale of 1: 200, and it corresponds to the full scale of 20 m x 20 m x 16 m as shown in Figure 1. This reduced scale model undergo the CFD simulation conducted by Ramponi and Blocken [12]. The result obtained was compared and accuracy was verified. In addition, the building model has a thickness of 2 mm and two windows facing each other in the centre of the windward and leeward façade [12]. Furthermore, the case studies were further modified based on the reference case. Figure 2 shows the building model used in this study, in which only the size of the inlet opening was changed. Table 1 shows the inlet and outlet opening sizes, together with the opening ratio in each case.

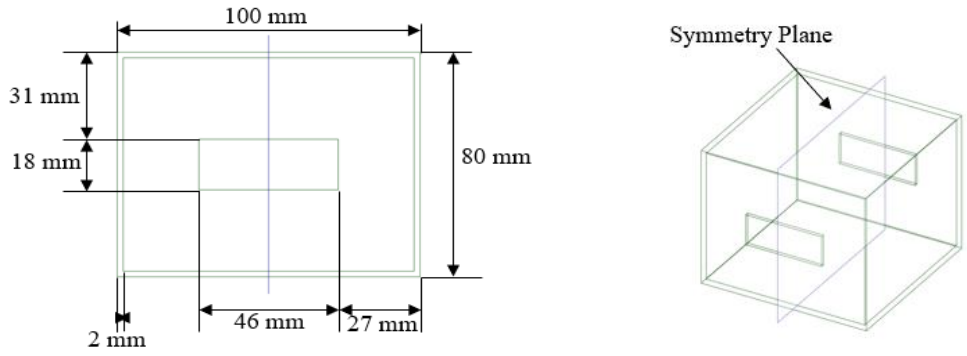

Figure 1. (a) Front view of model dimension and (b) Symmetry plane of reference building model

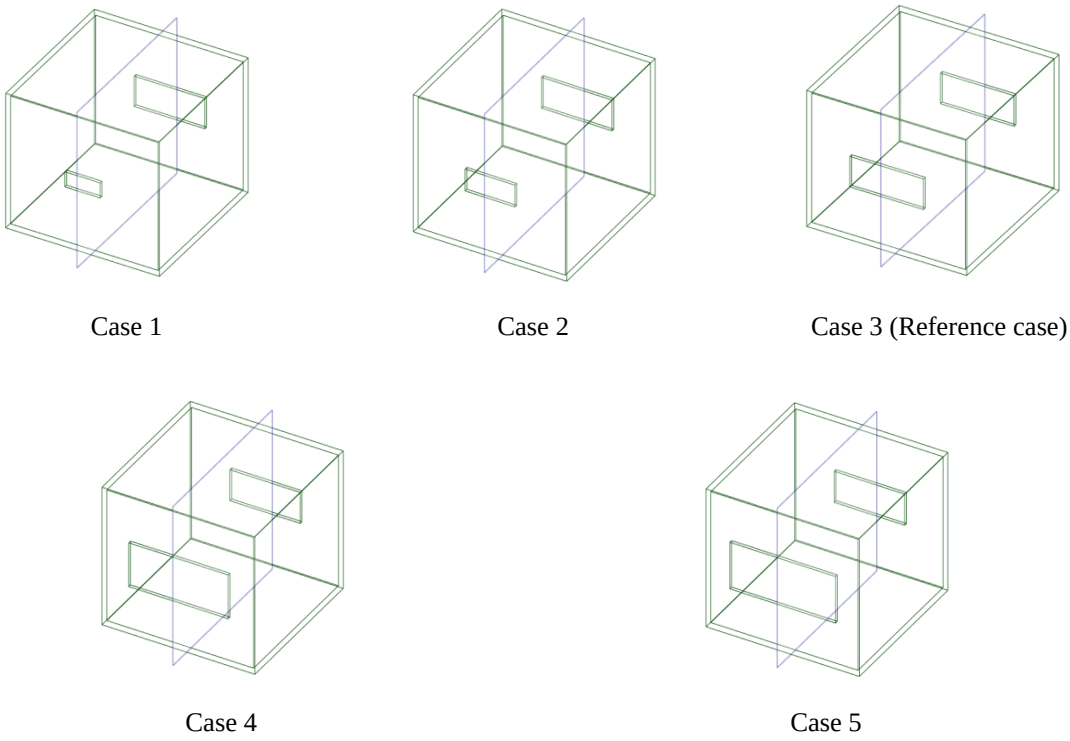

Figure 2. Isometric view for all five different cases

Table 1. Dimension of opening sizes and opening ratio for all five different cases

	Inlet Opening Size, mm (Width x Height)	Outlet Opening Size, mm (Width x Height)	Opening Ratio (Inlet to Outlet Ratio)
Case 1	23 x 9	46 x 18	1:4
Case 2	32.52 x 12.73	46 x 18	1:2
Case 3	46 x 18	46 x 18	1:1
Case 4	65.04 x 25.45	46 x 18	2:1
Case 5	69 x 27	46 x 18	9:4

Computational Domain

The computational domain created in this study was based on Ramponi and Blocken study [12]. This computational domain was created in order to generate the real flow field surrounding the building and around the window and to ensure the accuracy of the results. According to previous studies, the length of the windward facade was set to 3H, the length of the leeward facade was set to 15H, and the length of the top and sides were set to 5H, where H represents the reference building height, which is 80 mm [12-14]. The intention to fix the upstream at 3H is to restrict the occurrence of unexpected slope in the approach flow profile [12,15,16]. Hence, a computational domain with dimensions of 0.9 x 1.544 x 0.48 m^3 was generated. Figure 3 shows the computational domain and its dimension in an isometric view.

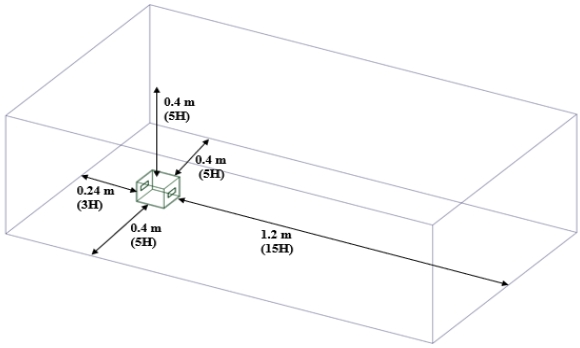

Figure 3. Dimension of the computational domain

Atmospheric Boundary Layer Condition (ABL)

According to Richards and Hoxey [17], the measured vertical profile of mean wind speed, turbulent dissipation rate and turbulent kinetic energy were used to define boundary conditions on the inlet plane in the simulation. In addition, a logarithmic law was used to define the inlet wind velocity profile, *U(z)*. The equation for the law of logarithm is shown in Eq. (1). The atmospheric boundary layer (ABL) friction velocity, u^*_{ABL} was calculated through Eq. (2), where the reference wind speed, U_{ref} = 6.97m/s, von Karman constant, κ = 0.4, aerodynamic roughness height, z_0 = 0.00003 m and the vertical height coordinate from the ground, z = 0.08m.

$$U(Z) = U^*_{ABL} \ln(\frac{z + z_O}{z}) \tag{1}$$

$$U^*_{ABL} = \frac{U_{ref \times k}}{\ln \frac{z + z_o}{z}} \tag{2}$$

The turbulent kinetic energy, *k(z)* in Eq. (3) was calculated by using mean wind speed, *U(z)* in Eq. (1), and measured streamwise turbulent intensity, $I_u(z)$. Previous studies have been conducted to identify the best value of parameter α. As recommended by Tominaga et. al., α = 1 was used in this study [12,13,14]. For the turbulent dissipation rate $\varepsilon(z)$, it was calculated by using Eq. (4). Through controlling the turbulent kinetic energy, *k(z)* and turbulent dissipation rate, $\varepsilon(z)$, specific dissipation rate, $\omega(z)$ was calculated through Eq. (5). The C_μ shown in Eq. (5) is an empirical constant that equals 0.09. For ground and building surfaces, standard wall functions developed by Launder and Spalding and sand-grain based roughness modification by Cebeci and Bradshaw's were used [18,19]. The values of roughness parameters, such as sand-grain roughness height, k_s and roughness constant, C_s were determined according to their relationship with the z_0 which has been obtained through the study of Blocken et al [15]. The ground sand-grain roughness height, k_s = 0.0006 m was obtained through Eq. (6) where the roughness constant, C_s was set at 0.5. The standard wall functions are also applied for building surfaces with k_s = 0.

$$k(z) = \alpha(I_u(z)U(z))^2 \tag{3}$$

$$\varepsilon(z) = \frac{(U^*_{ABL})^3}{k(z + z_o)} \tag{4}$$

$$\omega(z) = \frac{\varepsilon(z)}{C_\mu k(z)} \tag{5}$$

$$k_{s=} \frac{9.793 z_o}{C_s} \tag{6}$$

The zero static pressure was implemented to the outlet plane. For top and side façade boundary conditions, zero gradient and zero normal velocity conditions of all variables were applied. In other words, a zero sheared condition was implemented. At last, the symmetry type was fixed for the symmetry plane.

Solver Setting

The CFD simulation was conducted using ANSYS 2019 R3. In this study, the 3D steady-state RANS equation was solved in combination with the SST k-ω turbulence model. The k-ω SST turbulence model was chosen because it was able to obtain results similar to the PIV experiments conducted by Karava et. al. [20]. The material used in this study was air with a density of 1.225kg/m^3 and viscosity of 1.789×10^{-5} kg/ms. The boundary conditions for inlet, outlet, top, side, ground, symmetry, and model in this study were inserted according to the user-defined (UDF) ABL conditions. Moreover, the SIMPLE algorithm was selected for all simulations in this study. For the spatial discretization, Green-Gauss Node Based was selected to be used and also the second order has been assigned to pressure, momentum, turbulent kinetic energy, and turbulent dissipation rate [12,21]. The high order term relaxation and warped-face gradient correction were also chosen to improve the accuracy of the results. The initialization of this study was done under standard initialization. The convergence was expected to be achieved when all the scaled residuals were stable and reached a minimum value of 10^{-4} for *k*, and 10^{-5} for x, y, z, and ω.

Grid Sensitivity Analysis

In this study, grid sensitivity analysis with three different grids and cell counts was conducted to eliminate the discretization error. The three different grids and cell counts that were considered in the study was coarse grid (327609 cell counts), medium grid (657737 cell counts), and fine grid (813868 cell counts). The simulation was carried out by using the above three different grids and cell counts, and a graph of mean streamwise speed ratio (U/Uref) was drawn.

The U represent the 3D streamwise velocity vector and Uref = 6.97 m/s represent the reference wind speed. The grid sensitivity analysis was based on the mean streamwise wind speed ratio (U/Uref) along the centreline of the inlet and outlet opening. The obtained grid sensitivity analysis will then compare with PIV wind tunnel experiment results that have been conducted by Karava et. al. [20]. Figure 4 shows the mean streamwise wind speed ratio (U/Uref) along the centreline of the inlet and outlet opening. Through simulation, the results show that the fine grid with 813868 cell counts is closest to the PIV wind tunnel experiment results by Karava et. al. Hence, the fine grid was retained for further analysis.

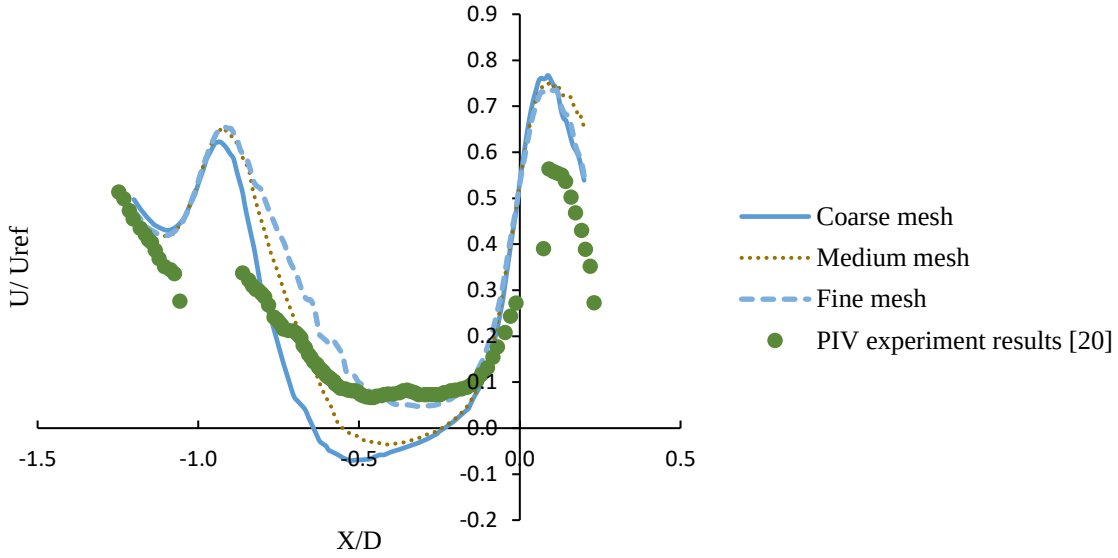

Figure 4. Simulation results from three different cell counts and PIV experiment results by Karava et. al. [20]

Model Validation

In this model validation section, the same building model reference case and turbulence model, namely the SST turbulence model were used to perform the simulation, and the obtained numerical simulation results were compared with those of Ramponi and Blocken, to verify the accuracy of the results [12]. The validation was done based on the velocity contour. As shown in Figure 5, the results indicate that the direction of air flowing from the inlet into the building model is downward, while the direction of air flowing out from the outlet of the building model is upward. In other words, a similar airflow trend was observed through the contour. Therefore, the reference case simulation result is considered acceptable since it shows a good agreement with the result obtained by Ramponi and Blocken.

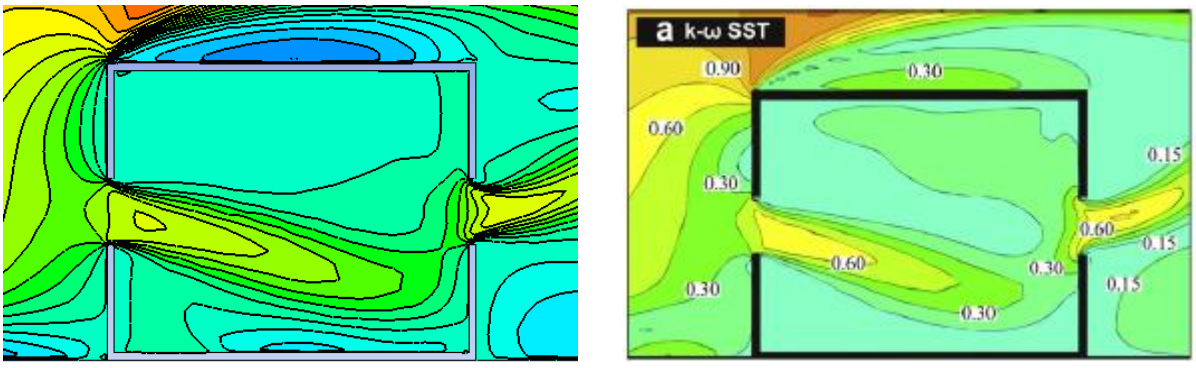

(a) (b)

Figure 5. Validation based on velocity contour: (a) Simulation result and (b) Result by Ramponi and Blocken [12]

RESULTS AND DISCUSSION

Velocity Vector

Figure 6 shows the velocity vector under various opening ratios. The velocity vector can be divided into two parts for discussion, namely the wind flow condition outside the building and wind flow condition inside the building. Regarding the wind flow conditions outside the building, it is noticed that three different recirculation zones are formed, which are located at the bottom of the windward wall, behind the leeward wall and at the roof of the building model. The incoming flow with a velocity of 6.97 m/s will hit the leading edge and leads to the flow separation. Due to the flow separation at

the leading edge, it is noticed that the flow is flowing over the building and into the building model as well as the bottom of the windward wall. The recirculation was also formed at the bottom of the windward façade. Moreover, when the flow is away from the building model, a reverse flow is generated, which will result in a larger recirculation behind the leeward wall and a smaller recirculation on the roof of the building model.

However, for internal flow, downward flow is observed when air enters the building model. In addition, when air passes through the building model, recirculation is formed above and below the airflow. Besides, when the outlet is larger than the inlet, the airflow will immediately be directed downwards until it hits the leeward wall. Then, the airflow is further divided into two parts. The first part will flow upward to the outlet opening and leave the building model, while the second part will flow downward and form a recirculate below the airflow. On the other hand, when the outlet opening is smaller than the inlet, the airflow will flow downwards first, and then flow upwards again when the airflow approaches the outlet opening. Due to the smaller outlet opening size, some of the air will flow downwards and form a recirculation below the airflow. Furthermore, when the air leaves the building model, an upward flow pattern is observed at the outlet. This flow will disrupt the recirculation behind the leeward wall, which will cause the recirculation to split into two parts.

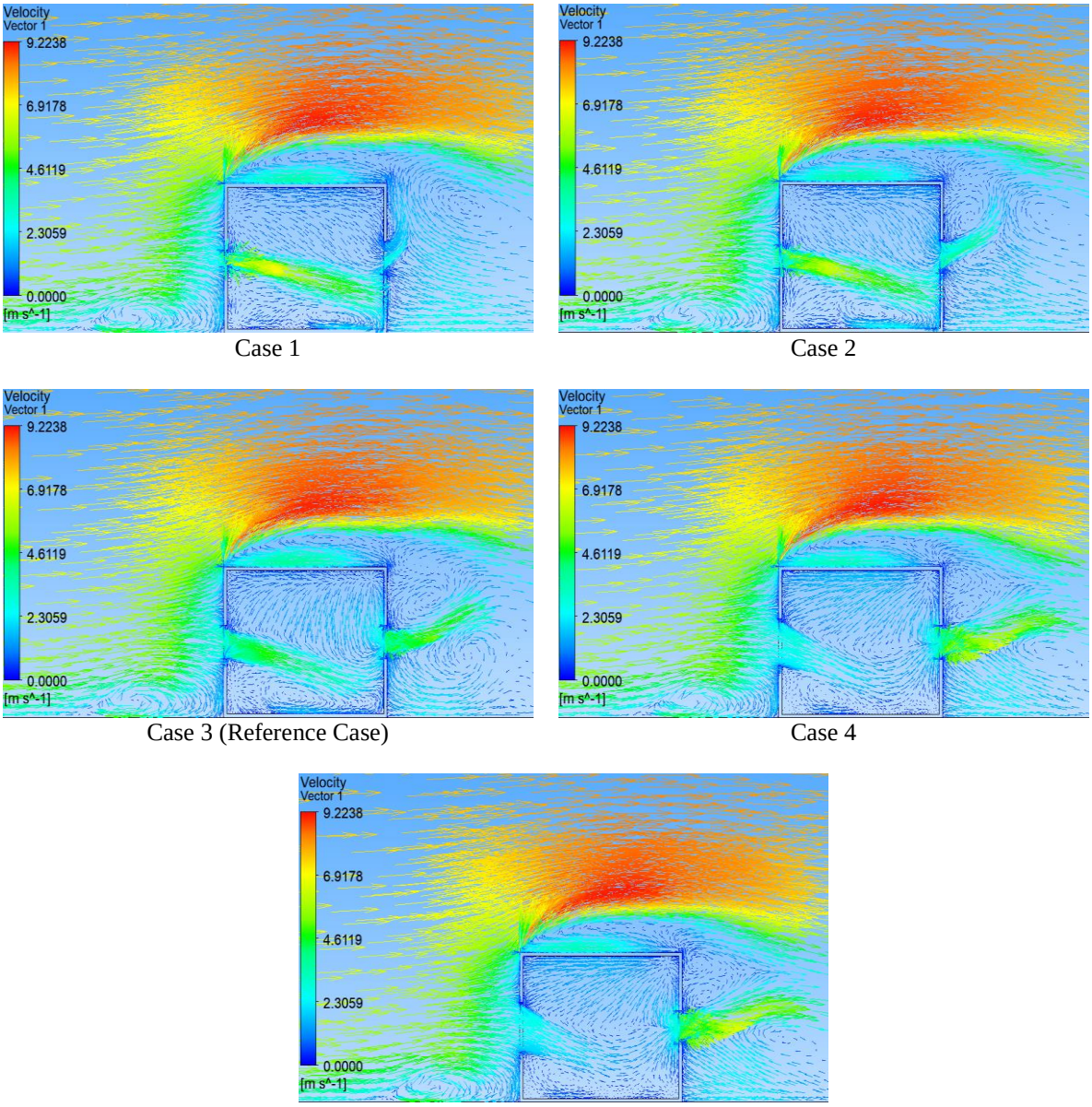

Figure 6. Velocity vector contours under different opening ratios

Velocity and Pressure

Figure 7 shows the contour of velocity and pressure under different opening ratios. Based on these contours, it clearly indicates that the internal air velocity increases as the opening ratio decreases. Moreover, as the opening ratio decreases, the pressure inside the building also decreases. The contour also illustrates that the results are in good agreement with Bernoulli's principle, that is, when the pressure inside the building model decreases, the velocity inside the building model

will increase. However, due to the different sizes of the opening at the inlet and outlet, this will result in different velocities and pressure at the opening.

Changes in air velocity entering the building in the larger opening ratio is relatively mild than a smaller opening ratio. Besides, the lower opening ratio will limit the volume of air entering the building and the air experience a sudden decrease in velocity when the air hits the windward wall. For this reason, it causes an increase in pressure around the opening. This increase in pressure forces the air into the building model at a high speed. This high speed will gradually decrease as the inlet size increases. Furthermore, the bigger outlet opening size than the inlet allows more air to leave the building model and lead to the decrease of pressure within the building model. As the inlet opening size keep increasing, the velocity at the outlet opening and pressure inside the building model is increased. Hence, case 1 has a higher velocity at the inlet opening but lower pressure and velocity inside the building model and outlet opening. However, case 5 having a lower velocity at the inlet opening but higher pressure and velocity inside the building model and outlet opening. Therefore, when the inlet opening size is larger than the outlet, the higher velocity is on the side with a smaller opening size, and vice versa.

Velocity Contour	**Pressure Contour**
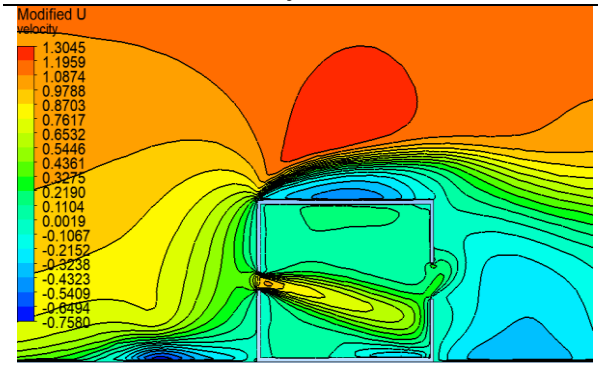	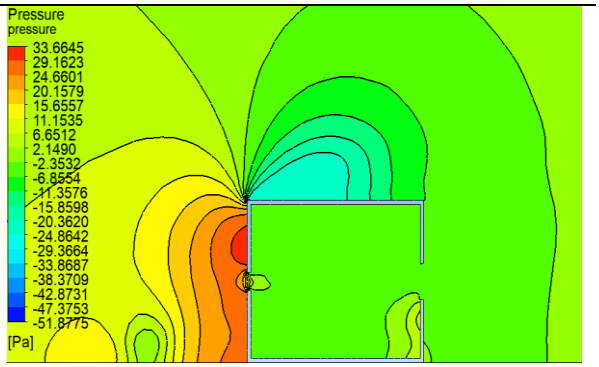

Case 1

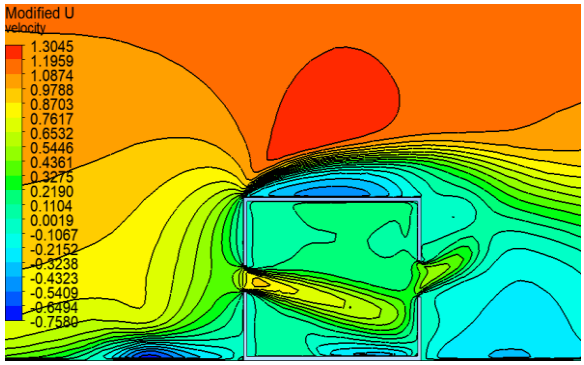

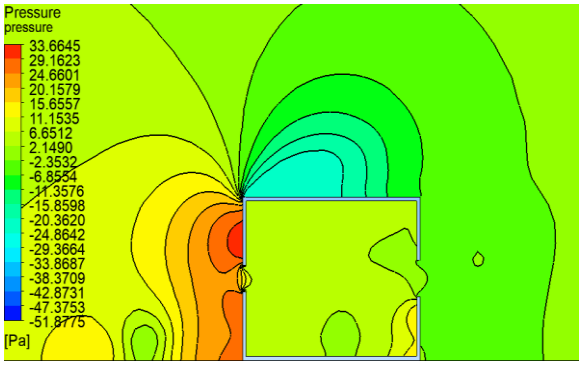

Case 2

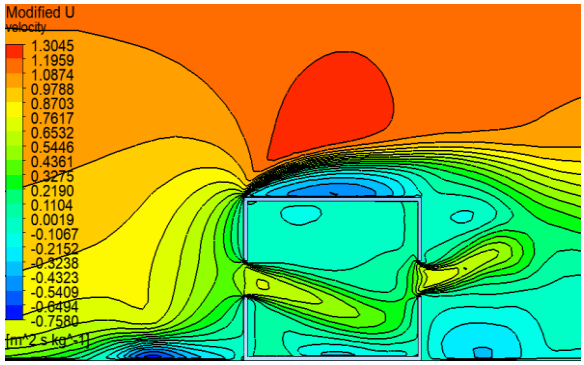

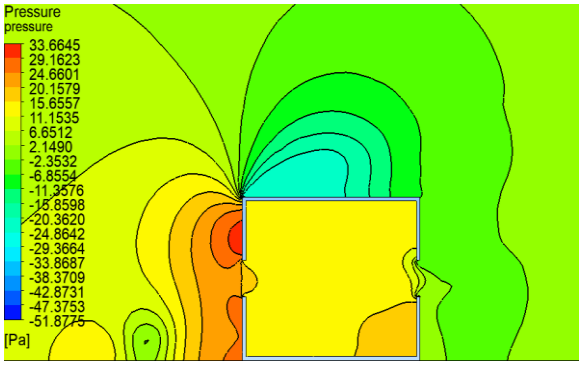

Case 3 (Reference Case)

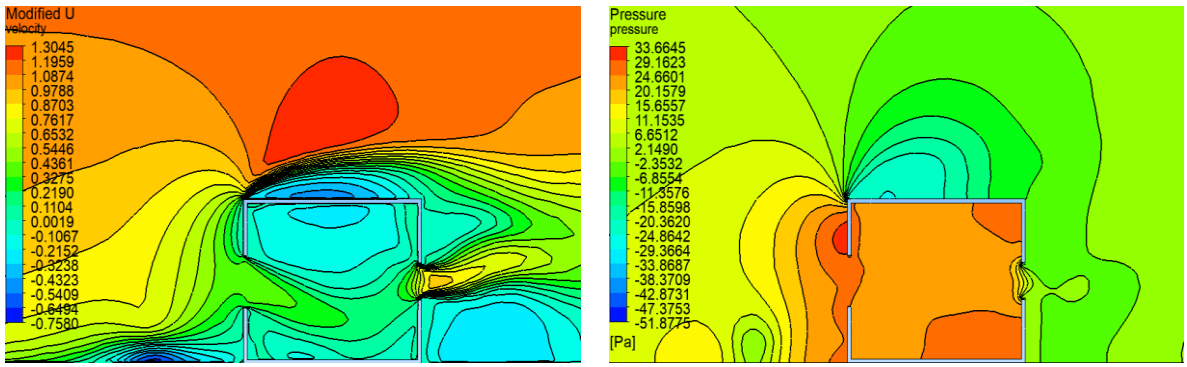

Case 4

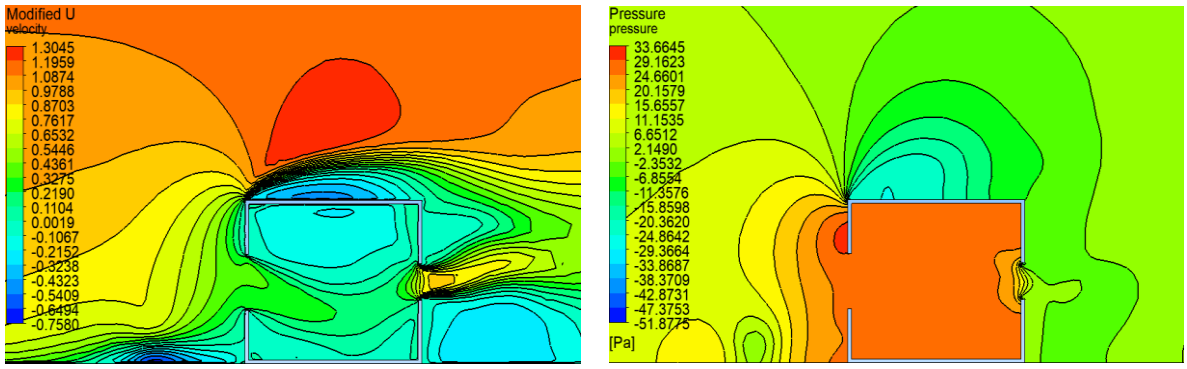

Case 5

Figure 7. Velocity and pressure contour under five different opening ratios

Pressure Drop

The Cp can be obtained through Eq. (7) where the density of air, $\rho = 1.225$ kg/m^3, and reference velocity, $V_{ref} = 6.97$ m/s, local building pressure, P, and reference pressure, P_r. Then, the ΔCp inside the building model can be calculated [22].

$$C_p = \frac{P - P_r}{\frac{1}{2}\rho V_{ref}^2} \tag{7}$$

According to Amanuel Tecle et. al, the lower the opening ratio, the higher the pressure drop, ΔCp inside the building model [23]. Through calculation, the results indicate that value of ΔCp increases when the opening ratio decreases. Based on Figure 8, it clearly illustrates that when the opening ratio is lower, e.g., 0.25 and 0.5, the pressure drop is higher, and when the opening ratio is higher, e.g., 2 and 2.25, the pressure drop is lower. In addition, the ΔCp between opening ratio 2 and 2.25 are getting smaller, further increase the opening ratio will result in a negative ΔCp. In this case, opening ratio 1 is located between higher and lower pressure drops. Therefore, from the obtained results, it is highly consistent with the results obtained by Amanuel Tecle.

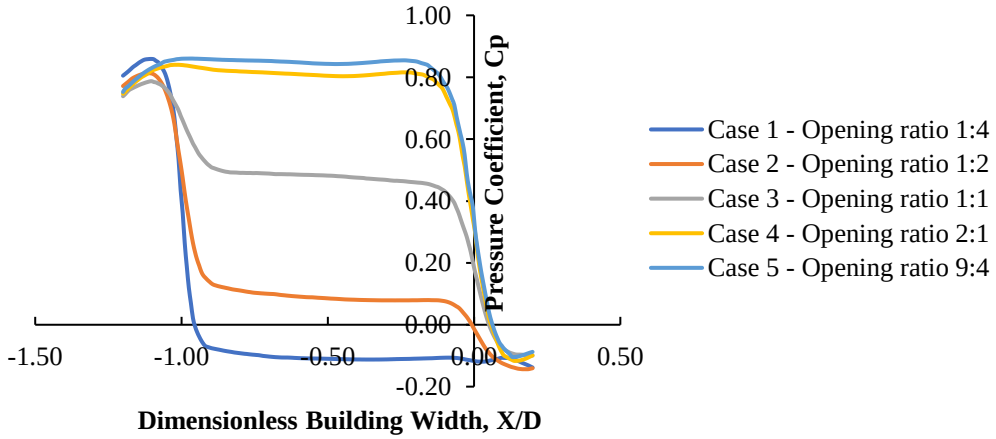

Figure 8. Pressure coefficient, Cp against dimensionless building width, X/D for five different opening ratios

Ventilation Rate

The ventilation rate for each case can be calculated through the following formula [22]:

$$C_Q = C_d \times V_{ref} \times (\Delta C_p)^{\frac{1}{2}} \tag{8}$$

$$C_a = \frac{C_Q}{1 + C_Q} \tag{9}$$

$$Q = C_a \times V_{ref} \times A_e \tag{10}$$

Flow coefficient, C_Q, can be calculated by using Eq. (8) with discharge coefficient, C_d = 0.62 and difference of pressure coefficient, ΔCp that has been discussed in the previous section. The actual flow coefficient, C_a was calculated by using Eq. (9). At last, the ventilation rate can be obtained through Eq. (10) with the effective opening area, A_e.

Figure 9 shows the ventilation rate when the inlet opening size is changed while the outlet remains constant. It can be clearly seen that the ventilation rate is initially increasing, but when the opening rate is greater than 1, it starts to decrease. Besides, it also illustrates that the highest and lowest ventilation rate is at case 3 and case 1, respectively. This phenomenon happens because case 1 has the smallest inlet which limits the volume of air entering the building model. Despite its large outlet, less air enters the building model, resulting in the lowest ventilation rate. When the opening ratio is greater than 1, the ventilation rate begins to decrease because the inlet opening size is larger than the outlet opening size. The larger inlet opening allows more air to enter the building model, but due to the smaller outlet opening size, it limits the volume of air leaving the building model. This leads to increased pressure inside the building model. In other words, when the opening ratio is less than 1, the percentage increase of ventilation rate is in the range of 40% to 90%. However, when the opening ratio is greater than 1, the percentage increase of ventilation rate ranged from -10% to 20%. Therefore, when the size of the inlet opening is larger than the outlet opening, this may cause air to accumulate inside the building, thereby causing a decrease in ventilation rate.

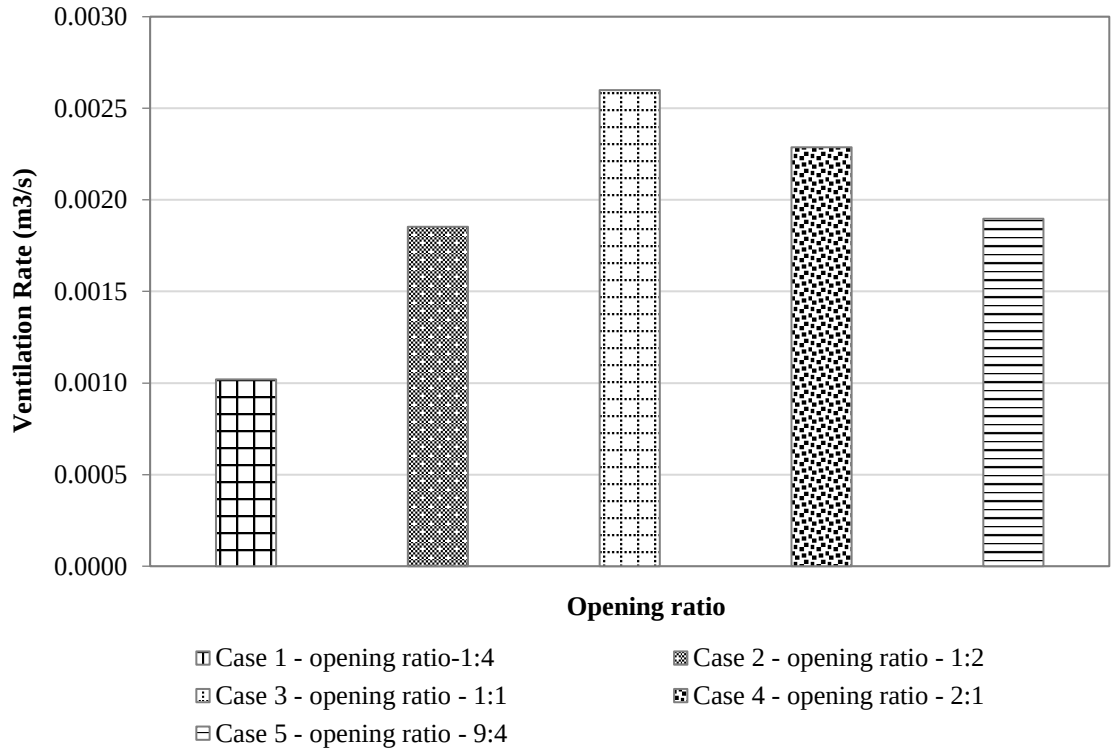

Figure 9. Ventilation rates under different opening ratios

CONCLUSIONS

In this study, the airflow characteristics in an isolated building and the influence of various opening rates on natural cross ventilation were investigated and analysed. In order to further understand the impact of cross ventilation, the numerical simulation based on the 3D-steady RANS equation was carried using five different inlets to the outlet opening ratios on the building model namely, 1:4, 1:2, 1:1, 2:1 and 9:4. The 3D-Steady RANS equation used in this study was solved associated with the SST k-ω turbulence model. The model validation and grid independence study were also performed and both showed great agreement with the results obtained by the previous study. The results of this study were discussed based on velocity vector, velocity and pressure, ventilation rate and ΔCp. Through velocity vector, it

illustrates that the recirculation was formed inside and outside of the building. For outside of the building, three recirculation were observed which was located at the bottom of the windward façade, behind the leeward façade and at the roof of the building model. However, as the air passes through the building model, the recirculation was formed at the top and bottom of the airflow. According to the result of velocity and pressure inside the building model, it is in good agreement with Bernoulli's principle, that is, the higher pressure leads to lower velocity. Moreover, when the outlet is greater than the inlet, the higher velocity was on the side with a smaller opening size and vice versa. For ΔCp, the results show that ΔCp increases as the opening ratio decreases. The results also illustrate that the ventilation rate was increased at first and then it started to decreases when the opening ratio was greater than 1. When the opening ratio was less than 1, the percentage increase of ventilation rate ranged from 40% to 90%. On the other hand, when the opening ratio greater than 1 the percentage increase of ventilation rate was ranged from -10% to -20%. Hence, the optimum ventilation rate can be said to be achieved when the opening ratio is 1:1. Therefore, it can be concluded that internal airflow was highly dependent on the opening ratio because the change in the size of the inlet opening greatly affects the performance of the ventilation rate. In future research, it is recommended to consider the incident angle of the wind, various wind speeds and various opening shapes to further understand the impact of opening on natural ventilation, thereby improving the performance of natural ventilation.

ACKNOWLEDGEMENT

The project is funded by the Ministry of Higher Education Malaysia, under the Fundamental Research Grant Scheme (FRGS Grant No: FRGS/1/2016/TK07/SEGI/02/1).

REFERENCES

[1] L. K. Moey, N. M. Adam, K. A. Ahmad, and L. C. Abdullah, "Wind tunnel study of different roof geometry configurations for wind induced natural ventilation into stairwell in tropical climate," *Int. J. Eng. Res.*, vol. 13, no. 5, pp. 2635–2647, 2018.

[2] N. Khan, Y. Su, and S. B. Riffat, "A review on wind driven ventilation techniques," *Energy Build.*, vol. 40, no. 8, pp. 1586-1604, 2008.

[3] WBCSD, "Energy efficiency in building. Business realities and opportunities, Switzerland, 2008.

[4] L. K. Moey, K. S. Goh, D. L. Tong, P. L. Chong, N. M. Adam, and K. A. Ahmad, "A review on current energy usage and potential of sustainable energy in Southeast Asia Countries," *J. Sustain. Sci. Manag.*, vol. 15, no. 2, pp. 89–107, 2020.

[5] T. S. Larsen, "Natural ventilation driven by wind and temperature difference," *Department of Civil Engineering, Aalborg University*, no. 2, 2006.

[6] I. Abd. Wahab., A. Kadir, and L. K. Ismail, "Opening design and position effect on building natural stack effect and cross ventilation," *Int. J. Eng. Res.*, vol. 5, no. 1, pp. 13–22, 2016.

[7] M. F. Mohamed, S. King, M. Behnia, and D. Prasad, "A study of single-sided ventilation and provision of balconies in the context of high-rise residential buildings," *World Renewable Energy Congress*, Linkoping, Sweden, 1954-1961, 2011.

[8] P. Karava, T. Stathopoulos, and A. K. Athienitis, "Wind-induced natural ventilation analysis," *Sol. Energy*, vol. 81, no. 1, pp. 20–30, 2007.

[9] T. Norton, J. Grant, R. Fallon, and D. W. Sun, "Assessing the ventilation effectiveness of naturally ventilated livestock buildings under wind dominated conditions using computational fluid dynamics," *Biosyst. Eng.*, vol. 103, no. 1, pp. 78–99, 2009.

[10] K. Visagavel and P. S. S. Srinivasan, "Analysis of single side ventilated and cross ventilated rooms by varying the width of the window opening using CFD," *Sol. Energy*, vol. 83, no. 1, pp. 2-5, 2008.

[11] L. K. Moey, Y. H. Sing, V. C. Tai, T. F. Go, and Y. Y. Sia, "Effect of opening size on wind-driven cross ventilation," *Int. J. Integr. Eng.*, vol. 13, no. 6, pp. 99–108, 2021.

[12] R. Ramponi and B. Blocken, "CFD simulation of cross-ventilation for a generic isolated building: Impact of computational parameters," *Build. Environ.*, vol. 53, pp. 34-48, 2012.

[13] J. Franke, A. Hellsten, H. Schlünzen, and B. Carissimo, "Best practice guideline for the CFD simulation of flows in the urban environment," *in 11th Conference on Harmonisation within Atmospheric Dispersion Modelling for Regulatory Purposes*, 2007.

[14] T. Yoshihide, A. Mochida, R. Yoshie, H. Kataoka, T. Nozu, M. Yoshikawa, and T. Shirasawa, "AIJ guidelines for practical applications of CFD to pedestrian wind environment around buildings," *J. Wind Eng. Ind. Aerodyn.*, vol. 96, no. 10-11, pp. 1749-1761, 2008.

[15] B. Blocken, T. Stathopoulos, and J. Carmeliet, "CFD simulation of the atmospheric boundary layer: Wall function problems," *Atmos. Environ.*, vol. 41, no. 2, pp. 38-252, 2007.

[16] B. Blocken, J. Carmeliet, and T. Stathopoulos, "CFD evaluation of wind speed conditions in passages between parallel buildings-effect of wall-function roughness modifications for the atmospheric boundary layer flow," *J. Wind Eng. Ind. Aerodyn.*, vol. 95, no. 9-11, pp. 941-962, 2007.

[17] P. J. Richards and R. P. Hoxey, "Appropriate boundary conditions for computational wind engineering models using the K-ϵ turbulence model," *J. Wind Eng. Ind. Aerodyn.*, vol. 46&47, pp. 145-153, 1993.

[18] T. Cebeci and P. Bradshaw, "Momentum transfer in boundary layers.," New York: Hemisphere Publishing Corporation, 1977.

[19] B. E. Launder and D. B. Spalding, "The numerical computation of turbulent flows," *The Comput. of Turbulent Flows*, vol. 3, no. 2, pp. 96-116, 1974.

[20] P. Karava, T. Stathopoulos, and A. K. Athienitis, "Airflow assessment in cross-ventilated buildings with operable façade elements," *Build. Environ.*, vol. 46, no. 1, pp. 266–279, 2011.

[21] T. Van Hooff, B. Blocken, and Y. Tominaga, "On the accuracy of CFD simulations of cross-ventilation flows for a generic isolated building: Comparison of RANS, LES and experiments," *Build. Environ.*, vol. 114, pp. 148–165, 2017.

[22] M. Swami and S. Chandra, "Procedures for calculating natural ventilation airflow rates in buildings," *ASHRAE Final Rep. FSEC-CR-163-86*, 1987.

[23] A. Tecle, G. T. Bitsuamlak, and T. E. Jiru, "Wind-driven natural ventilation in a low-rise building: A boundary layer wind tunnel study," *Build. Environ.*, vol. 59, pp. 275–289, 2013.